EFFECTS OF NON-LINEARITY ON THE FLAME RESPONSE AND CONTROL OF COMBUSTION INSTABILITIES IN A MATRIX BURNER

Dieter Bohn*[1], Nils Ohlendorf[2], James Willie[2]

[1] Institute of Steam and Gas Turbines, RWTH Aachen University
Templergraben 55, 52056 Aachen, Germany
[2] Institute of Steam and Gas Turbines, RWTH Aachen University
Templergraben 55, 52056 Aachen, Germany
* Corresponding author: post-bohn@idg.rwth-aachen.de

This paper discusses the effect of non-linearities inside a matrix burner on the flame response and control of instabilities inside the matrix burner. In particular, the response of the flame to high gain and frequency of the forcing signal are discussed. The importance of the choice of the combustion model used in the numerical simulation of combustion instabilities is highlighted. The effect of non-linearities on the choice of the primary fuel actuator that was used as active control device is discussed. Finally, it is shown that the occurrence of limit cycle behavior inside the combustor of the matrix burner led to hysteresis. The analysis begins with the discussion of the stability map of the matrix burner obtained from measurements.

1 Introduction

Gas turbines are designed to run in lean premixed prevaporized mode in order to limit temperatures and reduce NOx emissions. The problem is that running gas turbines near the lean flammability limit makes them exceptionally prone to combustion instabilities. One reason is that if combustion is near the lean blowout limit, small changes in the equivalence ratio due to the perturbation of the flow upstream can lead to periodic extinction. This action in turn leads to a larger fluctuation in the equivalence ratio at the flame, which in turn leads to fluctuation in the heat release rate. Hitherto, gas turbines were mostly operated with diffusion flames, but the high temperatures associated with such flames led to high NOx emissions. Combustion instabilities are not only common in gas turbines, but also in other combustion systems like rocket engines, jet engines, after burners, etc. If not checked it can lead to component failure and in the worst case to a catastrophic breakdown in the operation of such engines. These instabilities to a large extent occur when the acoustic modes of the combustion chamber couple with the combustion dynamics. In most cases, a feedback mechanism exist between the combustion process, the inlet conditions and the acoustic modes of the chamber. This is in part due to the fact that a time lag exist between the time a mixture is injected and the time it actually reaches the flame front and it has been shown that this time lag affects the combustion instability in gas turbines [1, 2]. This is true when this time is a multiple of the acoustic frequency of the combustor (or $\tau \cdot f_{acu} = 1, 2, 3, ...$). Putnam showed that there will be amplification in the pressure amplitude when these integers are off by a quarter cycle (0.25) or less [3]. In addition to this time lag, the vortex shedding frequency also effects the heat release frequency. This is because when a vortex is shed, mixing and scalar dissipation rates are significantly increased and therefore the local reaction rates are also increased.

Combustion instabilities are driven mainly by fuel/air equivalence ratio (ϕ) fluctuation and velocity perturbation [1,4,5]. These processes either directly or indirectly affect the pressure and the heat release

fluctuations inside the combustor. According to the Rayleigh criterion when the pressure and the heat release are in phase, instability is encouraged and when they are out of phase, the opposite is true [6]. Mathematically, this can be written as:

$$R = \int_V \int_0^\tau p'(x,t) q'(x,t) dt dV > 0. \tag{1}$$

In Eqn. (1), R is referred to as the Rayleigh index. This equation is a necessary, but not a sufficient condition for combustion instabilities to occur [7]. In order to realize the resonant effect in combustion systems, the acoustic energy of the system must exceed the dissipative effect in the system. The Rayleigh criterion was therefore modified by Chu, 1965 [8] in order to take this effect into account and can be written as:

$$\frac{\gamma - 1}{\bar{\rho} \cdot \bar{c}^2} \int_V \overline{p'(t) q'(t)} dV > \int_S \overline{p'(t) u'(t)} dS. \tag{2}$$

Another approach, apart from running gas turbines lean that is being adopted to address future restriction in gas turbine emissions is the use of combined-cycle power plants with efficiencies of 60% and higher [9].

This paper discusses the effect of non-linearities inside a matrix burner on the flame response and control of instabilities inside the matrix burner. In particular, the response of the flame to high gain and frequency of the forcing signal are discussed. The importance of the choice of the combustion model used in the numerical simulation of combustion instabilities is highlighted. In the work by [10], it was shown that this decision can affect the results obtained in the CFD simulation of thermoacoustics. The non-linearities in the matrix burner also affected the choice of the primary fuel actuator that was used as active control device for suppressing the instabilities. In particular, for high equivalence ratios, the non-linear effect led to saturation of the proportional injector, which led to it loosing its actuation authority. However, when an "on-off" saturated valve was used, suppression of the instabilities inside the matrix burner was possible, although secondary peaks were visible in the pressure spectrum of the controlled combustor. Similar observation was made and reported in the work by [11, 12]. The occurrence of low and high frequency secondary peaks are attributed to the coupling of the components of the controller with the dynamics of the combustor.

Systems exhibiting non-linear limit cycle behavior are prone to bifurcation and hysteresis. Such systems are capable of keeping a memory of themselves. This is true for gas turbine burners that exhibit thermoacoustic instabilities. It is believed that the limit cycle behavior inside the matrix burner also gave rise to this effect. Hysteresis has been reported in the work by [13–17]. Their investigated configurations were different but certain similarities can be found in their results. For example, Lieuwen [13] investigated a premixed swirl stabilized combustor while Matveev et. al. [17] investigated an electrically heated grid Rijke tube. In general, however, hysteresis can be attributed to either changes in the air mass flow or to changes in the fuel mass flow. The latter was investigated for the matrix burner in this paper. The approach used in this work is similar to that used in the work by Isella et. al. [14]. The matrix burner investigated here is similar to that investigated by Deuker [18] and Krüger [19].

2 Experimental Setup

The experimental set up of the test rig is shown in Fig. 1. The test rig was designed to study self-excited thermoacoustic instabilities. Additionally, the rig has been equipped with a fast response injector and a loudspeaker for active combustion instabilities control.

The test rig consists of air and fuel supply systems, an ignition or pilot flame, and a premixing chamber. Once ignition is over, the pilot flame is switched off. It is also used in the modulation of the secondary fuel for active control. Upstream propagation of the flame is prevented by a 2D matrix element, which has seven slots, each measuring 2.5 mm x 40 mm in cross-section and 50 mm in height as shown in Fig. 1. The air inlet pipe is a DN 50 pipe with an inner diameter of 54.5 mm. The test facility is equipped with sensors and instruments for measuring the air and the fuel mass flow rates, pressure, temperature, heat release and emissions.

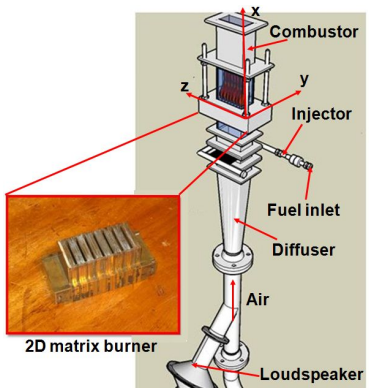

Figure 1: Sketch of the test rig used in measurements.

Air enters the test rig at the air inlet (see Fig. 2) and a honey comb is placed downstream to streamline the air flow. The air leaving the honey comb flows through a diffuser that lowers the air velocity and decreases the pressure loss across the burner. Fuel enters the mixing chamber first through the main fuel pipe (of diameter 17 mm) that is connected to nine smaller pipes of diameter 4 mm at right angles to the main fuel inlet pipe. Each of the nine pipes has four inlet fuel holes of diameter 2 mm that leads to the mixing chamber. The fuel inlet is choked because of the large pressure drop (Δp) across it. Fuel is admitted in an opposite direction to the direction of the air flow. Due to the turbulence caused by this counterflow and the velocity difference between the fuel and the air, mixing is improved. This is because of the increase in the residence time of the mixture in the mixing chamber. This mode of injection was employed in the early design of gas turbine burners like the Bristol Siddeley Gyron Junior [20]. Before the mixture enters the 2D slots from the mixing chamber, the test rig is fitted with a silica glass window of length 60 mm and it is also fitted with same glass window at the exit of the burner matrix inside the combustor to allow optical measurements like PIV, LDA and heat release measurements using a photomultiplier (PMT) that is combined with an OH*-Filter. Three PMTs are used for simultaneously measuring the OH*, CH* and C2* radicals that are used as an indicator for heat release. The primary fuel is modulated by the use of an actuator (a fast response injector) that is discussed in details later in the paper. It is mounted on the main fuel inlet pipe and denoted as "injector" in the sketch in Fig. 1. The combustion chamber has a cross section of 92 mm x 46 mm and add-ons that makes it possible for variable combustor lengths of 200 mm, 400 mm, 600 mm, 800 mm and 1000 mm. The outlet of the combustor is connected to a flexible tube of length 6 m that exhausts the combustion products to the atmosphere. A transition piece connects the combustor outlet to the flexible tube.

The combustion air is supplied by a screw compressor at constant pressure and the fuel (propane) is taken from gas cylinders. Both flow rates can be adjusted and determined separately. The air and fuel flow rates are measured through a laminar mass flow meter within an accuracy of $\pm 5\%$. The exhaust gas temperature is measured using a PtRh-Pt thermocouple. The combustion chamber is surrounded with mineral wool to reduce thermal losses because it was not air or water cooled. However, most gas turbine burners that have been reported in the literature are air cooled. Radiation losses were still present through the silica glass window and the chimney. The combustor was operated at equivalence ratios between 0.69 and 1.6. In order to obtain information on the acoustic instability of the combustor, the pressures inside the combustor and mixing chamber are measured using probe microphones and recorded using dSPACE.

3 CFD Model Setup

Model abstraction is critical in CFD simulation because of the need of simplification of the analysis, but at the same time the physics of the problem must be captured. In the case of the matrix burner test

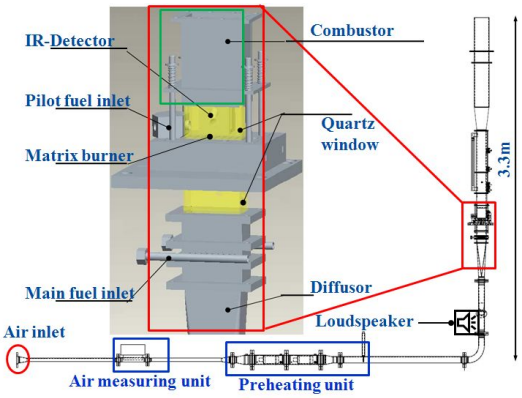

Figure 2: Schematic of the matrix burner.

rig investigated in this work, for example, the detailed fuel inlet was not included in the geometry that was simulated because it is choked. To limit the size of the computational grid, the ducts at the inlet and outlet are not included in the computational mesh. The approach in this case is to determine their impedances and superimposed them on the CFD simulation as discussed in details in [21].

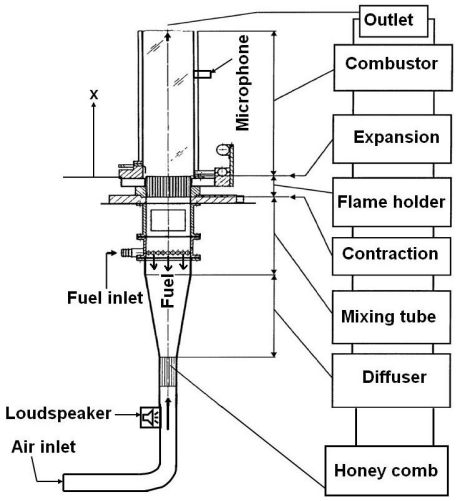

Figure 3: Model of the matrix burner test rig.

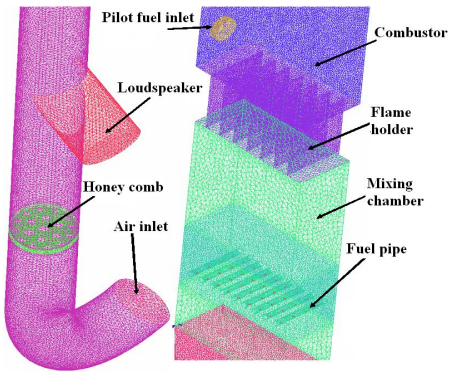

Figure 4: CFD surface mesh of the test rig.

The CFD model simulated for the test rig is shown in figure 3. The CAD drawing of the test rig was done using Pro/Engineer and the mesh was generated using ICEM CFD. The mesh was unstructured and tetrahedral. For the sake of clarity, the surface mesh, with no volume, cut in to two, is shown in figure 4. The mesh size is 2.4 million cells.

3.1 Solver and Boundary Conditions

The Fluent 6.3 pressure based couple solver was used. For discretizing the governing equations the QUICK scheme was used. Time matching was done implicitly using a second order scheme. For turbulence modeling, the k – ε realizable model was used. This model uses the assumption of eddy viscosity and the resulting turbulent transport equation that is solved is diffusive, which makes it much more easier to handle than other turbulent models like the Reynolds stress models.

Four parallel processes, each using a total of two processors on a Linux cluster at the RWTH Aachen

University high performance computing center were used for the numerical simulations. The CPU is an AMD Opteron 885 that has a 2.6 GHz (dualcore) processor with a memory of 32 GByte per node.

The CFD boundaries are as follows: the air duct is given a velocity inlet boundary and the combustor outlet is treated as a pressure outlet. The rest of the surfaces are treated as walls with no slip and adiabatic conditions. The fuel inlet is a mass flow inlet. The acoustic boundary conditions implemented in Fluent are time invariant, thus making them less suitable for acoustic applications. Acoustic boundaries must vary with time to account for the movement of acoustic waves. This problem is solved by using UDFs as explained in the work by Bohn et.al [21] and Schuermans et. al [22].

3.2 Combustion Model

The species transport equation or the balance equations for the mass fraction of species i can be written as:

$$\rho \frac{\partial Y_i}{\partial t} + \rho \mathbf{u} \cdot \nabla Y_i = -\nabla \cdot \mathbf{j_i} + \omega_i, \tag{3}$$

where i=1,2,3,.....n. The left hand side terms represents the local rate of change and convection. The first term on the right hand side is the diffusion flux denoted by $\mathbf{j_i}$ and the last term is the chemical source term, which is unclosed. It is closed by using two combustion models and the results obtained compared. In one case, the combined finite rate/eddy dissipation model is used [23]. This model determines the Arrhenius rate and the eddy dissipation rate and picks the smaller of the two as the net rate of reaction. The assumption of a one step irreversible reaction is used. It is of the form:

$$\nu'_F F + \nu'_O O \rightarrow \nu'' P, \tag{4}$$

where F is the fuel and O is the oxidizer. In the eddy dissipation model, the rate of the reaction is given by $\omega = \min(\omega_1, \omega_2)$, where ω_1 and ω_2 are given by:

$$\omega_1 = \nu' W_R A \rho \frac{\epsilon}{k} \min_R \frac{Y_R}{\nu'_R W_R}, \tag{5}$$

and

$$\omega_2 = \nu'' W_P A B \rho \frac{\epsilon}{k} \frac{\sum_P Y_P}{\sum_K^N \nu''_R W_P}. \tag{6}$$

A and B are empirical constants equal to 4.0 and 0.5 respectively.

In the finite rate chemistry model, the Arrhenius rate of reaction is given by:

$$\omega = B \rho \frac{Y_F}{W_F} \rho \frac{Y_{O2}}{W_{O2}} \ exp\left(\frac{-E}{RT}\right). \tag{7}$$

Critical is the determination of the parameters E and B since the values reported in the Fluent solver are for stoichiometric conditions. To determine these values for an equivalence ratio of 0.59 that was used in the CFD simulations, kinetic data in the work by [24, 25] are used. The values of B and E determined are 2.03 x 10^8 J/(kmol) and 2.40 x 10^{13} m^3/(kmol s) respectively. The rate exponents for both fuel and oxidizer in the second order reaction used are set to unity.

4 Results and Discussions

4.1 Heat Release Dynamics in the Matrix Burner

The dominant process that contributes to heat release perturbation in the matrix burner is due to a thin-wrinkled flame [23]. In this case, the flow is mildly turbulent which leads to a smaller chemical time scale when compared to the turbulent time scale ($Da > 1$, which implies that the reaction is mixing limited).

The flame surface area in this case is characterized by a single value function $\xi(t)$ that represents the instantaneous axial displacement of the flame, which can be written as:

$$\frac{\partial \xi}{\partial t} = u - v\frac{\partial \xi}{\partial r} - S_L(\phi)\sqrt{\left(\frac{\partial \xi}{\partial r}\right) + 1}, \tag{8}$$

and the total heat release Q is proportional to the integral of this surface over an anchoring ring, which can be written as:

$$Q = \kappa(\phi)\int_0^R \sqrt{1 + \left(\frac{\partial \xi}{\partial r}\right)^2}\, dr, \tag{9}$$

where S_L is the burning velocity, $\kappa(\phi) = 2\pi\rho_u S_L(\phi)\Delta h_r(\phi)$, ρ_u is the density of the unburnt mixture and Δh_r is the heat of reaction. Equation (9) clearly suggests that fluctuation in the flame surface area can lead to heat release fluctuation. Similarly, fluctuations in density, flame speed and heat of reaction can also lead to heat release perturbation. In the matrix burner, the non-linear coupling is predominantly between the equivalence ratio and the heat release fluctuations. The fluctuation in the equivalence ratio is driven by fluctuation in the air flow rate since the fuel inlet is choked. This observation was proven from the stability map that is discussed below. There is some perturbation in the velocity at the exit of the burner, but this is small in comparison to the equivalence ratio fluctuation. Sensitivity analysis carried out by Deuker supported this observation [18]. In thermoacoustics, the flame acts as an active monopole source of sound. Observations have shown that for the matrix burner, in addition to the above mentioned, the flame is also acting as an autonomous source of sound, leading to the generation of noise, which is a random process, unlike acoustics, which is deterministic. This action was mainly driven by the interaction between the flame fronts in the matrix burner as shown in Fig. 5. It remains unclear whether the flame front interaction inside the matrix burner created a feedback mechanism that contributed to the thermoacoustic instability. Observation, however, showed that during the flapping action, the flame surface area fluctuates which could lead to fluctuation in the heat release dynamics. The stable flame in this figure shows no interaction between the flame fronts whereas in the unstable flame, this interaction can be clearly seen. Another observation is that the stable flame is shorter in length than the unstable flame.

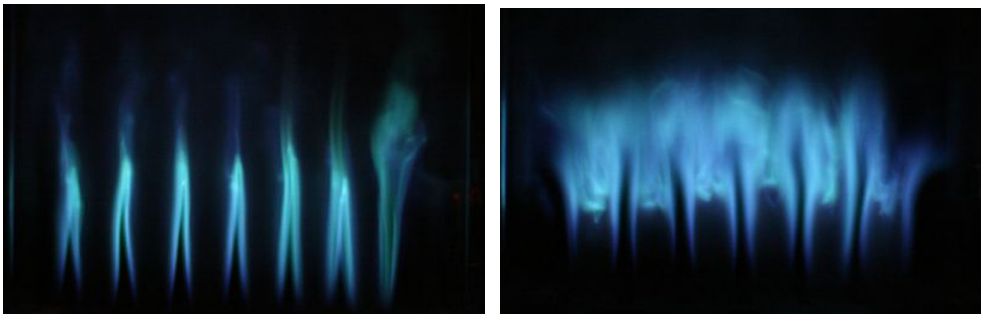

(a) Stable flame (b) Unstable flame

Figure 5: Stable and unstable flame of the matrix burner, $\bar{\phi} = 0.86$, air mass flow = 6.93 g/s.

4.2 Stability Map of the Matrix Burner

The stability map obtained from measurements for the matrix burner is shown in Fig. 6. It has been previously reported in the work of Deuker [18] and Bohn and Deuker [26]. In this case, the test rig was run at fuel/air equivalence ratios in the range $\phi \in [0.4, 1.54]$. For the range $0.4 \leq \phi < 0.44$, the matrix burner experienced transition. For values of the equivalence ratio in the range $0.44 < \phi < 0.67$, the matrix burner was mostly quiet, even though there were instances where it showed some transition behavior. For the

range of ϕ values between 0.67 and 1.25 (i.e, $\phi \in (0.67, 1.25]$), the matrix burner was unstable and experienced strong oscillations. Finally, for ϕ>1.25, the burner was mostly stable, even though it showed transition behavior at ϕ=1.33 and became unstable again at ϕ=1.43.

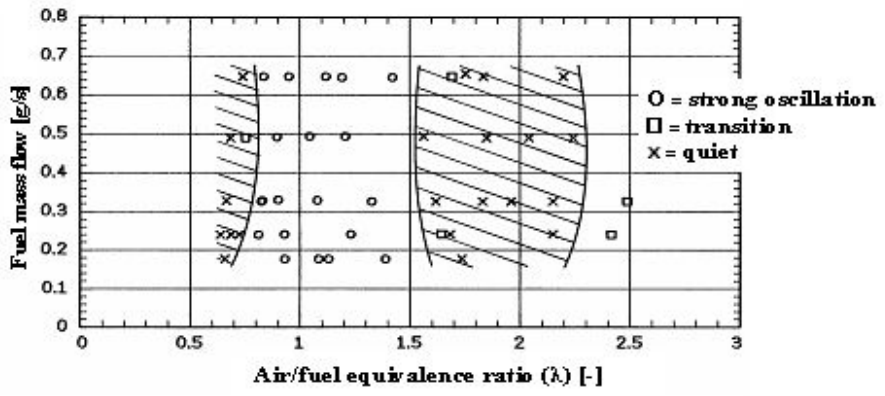

Figure 6: Stability map of the matrix burner taken from [18]

One major finding from the stability map is that to move from stable to unstable behavior or vice versa, the fuel mass flow rate is kept constant while the air mass flow rate is changed. When the opposite is done (i.e, keeping air mass flow fixed and changing the fuel mass flow rate), this behavior will not be realized from the stability map. This is one proof that the coupling of the acoustic of the combustion chamber with the inlet conditions is from the air side, mostly referred to as air-side coupling.

4.3 Comparison of Combustion Models

Self exciting simulations are performed using the finite rate chemistry model and the combined finite rate chemistry/eddy dissipation model. The air inlet velocity was 40 m/s and the equivalence ratio was 0.59. The length of the combustion chamber was 400 mm. The temporal variation of the pressure in the plane x=140 mm are plotted in Figs. 7(a) and 7(b) for both combustion models. The time series data shows linear growth, exponential growth followed by the limit cycle, which is an indication of saturation and nonlinearity in the matrix burner. In such cases, there are conditions for the existence and stability of nonlinear periodic motion, which is otherwise referred to as super-critical bifurcation. Significant, however, is the fact that the pressure predicted by the finite rate chemistry model is higher than that predicted by the combined model. Even though the combined model computes both the Arrhenius rate and the eddy dissipation rate, the net rate of the reaction is the smaller of the two and this is almost always taken as the eddy dissipation rate after ignition. Before ignition, however, the rate of reaction is the Arrhenius rate. The temperature sensitivity of the Arrhenius or finite chemistry rate makes it to shoot up after ignition. The eddy dissipation model is numerically dissipative and it also does not account for chemistry. For this reason, for example, it is unable to capture the variation of the flame speed with equivalence ratio, something the finite rate chemistry model can do.

The flames of the two models after a computational time of 0.2093 s are as shown in Fig. 8. The difference in flame length and shape are clearly visible. In the case of the finite rate chemistry model, the temperature is higher and the length of the flame is shorter than it is for the combined model. The length of the flame, for example, determines the flame Strouhal number, which can be defined as $St = f l_f / u_0$, where f is the frequency, l_f is the flame length and u_0 is the mean velocity at the burner mouth. This number in turn determines the behavior of the flame transfer function.

Even though the unstable frequency predicted by both models were closed (563 Hz for the combined model and 621 Hz for the finite rate chemistry model), the difference in amplitudes are significant (6.44 x 10^5 Pa for the combined model and 2.59 x 10^7 Pa for the finite rate chemistry model).

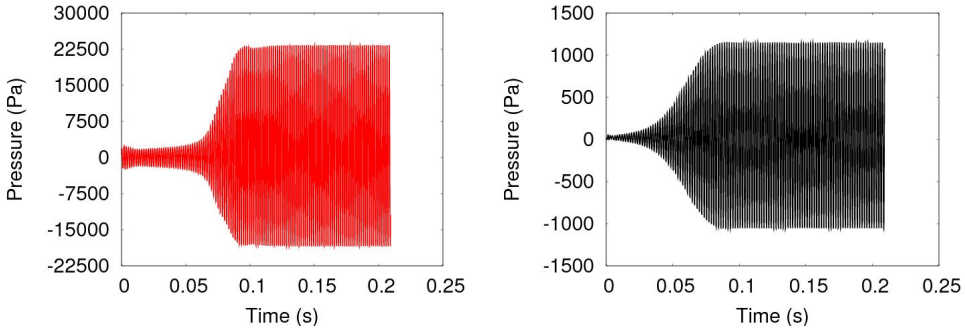

(a) Finite rate chemistry model (b) Combined model

Figure 7: Pressure time series inside the combustion chamber, $\phi = 0.59$, air inlet velocity = 40 m/s.

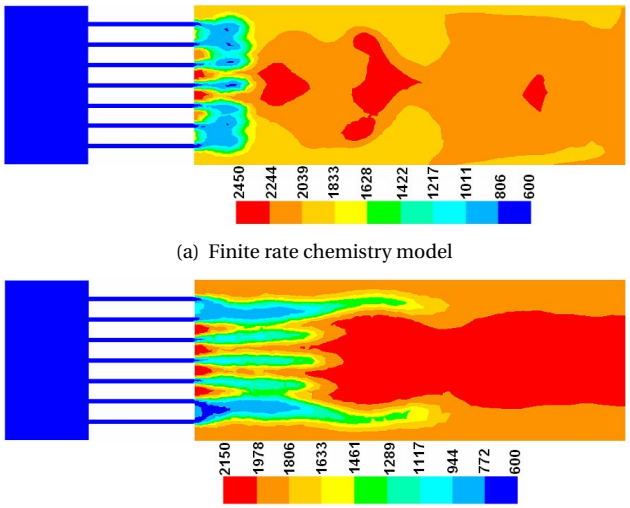

(a) Finite rate chemistry model

(b) Combined model

Figure 8: Temperature(K) in the plane z=0, $\phi = 0.59$, air inlet velocity = 40 m/s.

4.3.1 Response of the Flame to Periodic Forcing of the Inlet Air

The response of the flame to a single frequency forcing at the velocity inlet is investigated for both changes in the frequency at constant gain and changes in the gain at constant frequency. The forcing is implemented in a UDF that was hooked at the air inlet. The UDF is of the form $u = \bar{u} + u_0 sin(\omega t)$, where $\omega = 2\pi f$ is the angular frequency in rad/s, u_0 is the gain and $\bar{u}$=40 m/s is the mean velocity at the air inlet. Unsteady simulations are performed at forcing frequencies of 81 Hz, 243 Hz, 405 Hz, and 567 Hz while keeping the gain fixed at 4 m/s. Time series data is written for 3000 time steps. The spectrum of the pressure for these frequencies in addition to the case without forcing are shown in Fig. 9. The forcing did not lead to a shifting of the dominant unstable frequency at 560 Hz but other significant multiple peaks are produced at other frequencies.

To test for nonlinearities the CFD simulations are repeated for a constant forcing frequency of 243 Hz but with different values of the gain such that $u_0/\bar{u} = 15\%$, $u_0/\bar{u} = 20\%$, $u_0/\bar{u} = 25\%$ and $u_0/\bar{u} = 30\%$. A system is defined as linear or non-linear in terms of the system excitation and response. As a rule, a linear system must satisfy the properties of superposition and homogeneity. One way to test for nonlinearities is by varying the gain of the input signal. The CFD simulations are performed for 3000 time steps and the spectrum of the pressure obtained inside the combustion chamber is as shown in

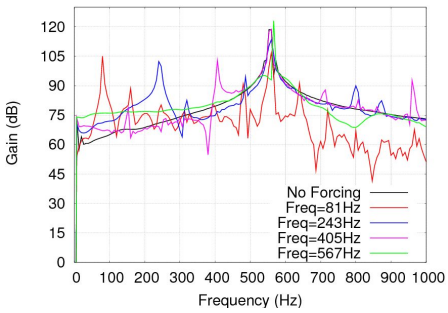

Figure 9: Spectrum of pressure inside combustor for varying forcing frequencies, $\phi = 0.59$, air inlet velocity = 40 m/s.

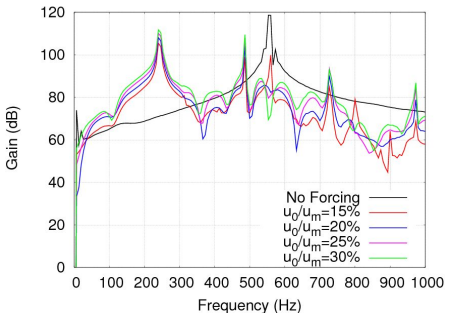

Figure 10: Spectrum of pressure inside combustor for different forcing amplitudes, $\phi = 0.59$, air inlet velocity = 40 m/s.

Fig. 10 together with the spectrum for the case when no forcing was applied. In the cases considered, the effect of changing the gain is pronounced because for the $u_0/\bar{u} = 15\%$ case, a single frequency forcing results in multiple frequency responses with almost equal gains at 560 Hz, 487 Hz and 240 Hz. For the rest of the cases, there is a complete shift in the unstable frequency from 560 Hz to 487 Hz and 240 Hz. Clearly, the system is not obeying the principle of superposition and therefore, it is nonlinear.

5 Effect of Non-Linearity on the Choice of the Fuel Actuator

One of the key questions in the control of combustion instabilities using fuel forcing is the choice of the actuator. In general, a proportional or an "on-off" valve can be used. To suppress the instabilities inside the matrix burner, a proportional injector was first investigated. This injector, however, was unable to suppress the instabilities due to the loss of its actuation authority. This could be attributed to the saturation or non-linear behavior of the matrix burner. A similar observation was reported by [11, 12] in which a proportional valve was successfully used to suppress the instabilities when the gas turbine test rig was operated in the linear regime at low equivalence ratios. However, when the rig was operated within the non-linear regime at higher equivalence ratios, the proportional valve could not suppress the instabilities in the system, but an "on-off" valve was able to suppress the instabilities.

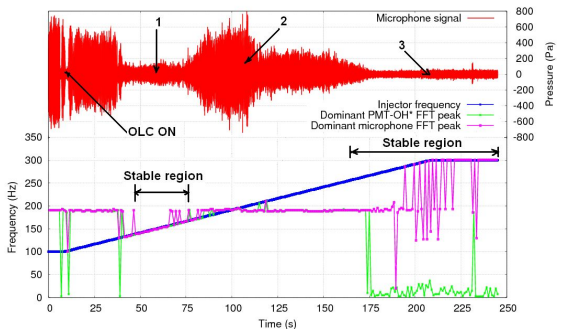

Figure 11: Time signal of microphone inside combustion chamber with and without pulsed primary fuel injection

In the matrix burner that was investigated in this work, an "on-off" injector by Bosch GmbH that works in the saturated mode was used for suppressing the instabilities in the matrix burner. The bandwidth of the injector was 300 Hz. The injector model is NGI2-CP and it was operated at 14 Volts. The high voltage ensured that the actuation action of the injector was very fast in order to prevent depletion of the fuel at the flame front as a result of the modulation of the primary fuel. This type of injector is

used mostly for automotive applications. The injector was installed behind a mass flow controller working with a time constant of 300 ms. The controller ensured that the mean fuel mass flow was constant within a given time frame by adjusting the injector admission pressure. The case considered was for an air mass flow rate of 6 g/s and an equivalence ratio of 0.86 g/s. The plot in Fig. 11 shows the time series signal recorded by the microphone for cases where the primary fuel injector was pulsed at various frequencies. Also shown in the plot are the injector frequencies, the dominant microphone frequencies and the dominant OH* signal frequencies. In some cases, secondary peaks were observed but only the dominant peaks are reported here. The injector frequencies were increased at a rate of 1 Hz/s beginning from 100 Hz. At the start, when the fuel was not modulated, the system oscillated at a frequency of 190 Hz with peak to peak pressure of 560 Pa. Modulating the fuel mass between (130-170) Hz shown in the figure as "line 1" almost completely suppressed the self-exciting oscillations. Similarly, primary fuel modulation in the frequencies range (265-300) Hz shown as "line 3" in the figure completely attenuated the instability. The microphone pressure dropped from 550 Pa to about 60 Pa. The observation through the quartz glass window showed that the flames tip went from turbulent to almost perfect "v-shaped" flames. For injector forcing frequencies above 265 Hz, secondary peaks at lower frequencies were visible in addition to secondary peaks at the forcing frequencies. In most cases, the amplitude at the lower frequencies were higher than those at the injector forcing frequencies. The frequency ranges (100-130) Hz and (170-265) Hz, shown as "line 2" in the figure were not able to suppress the instabilities inside the combustor. It seems that they were too close to the fundamental unstable frequency of the combustor (that is, 190 Hz) at this operating point.

6 Effect of Equivalence Ratio Variation on Pulsations and Temperature

The effect of variation of the equivalence ratio (ϕ) on pulsations levels in the matrix burner was investigated for two cases. In one case, the average air mass flow rate was keep fixed at 6 g/s and in the other, the average air mass flow rate was kept fixed at 8 g/s. In the two cases considered the fuel mass flow rate was varied by increasing it at a rate of 0.02 g/s. It was observed that when the mean ϕ was increased gradually, the system moved from stable to unstable and when the mean ϕ was decreased gradually, it went from unstable to stable at the same mean value of ϕ close to 1.3 for the 6 g/s air mass flow case. This observation was seen in the 8 g/s case but it was not pronounced. One reason for this sudden bifurcation in the system is hysteresis. For each equivalence ratio considered, the temperature and pressure were monitored. The stability map based on the root mean square pressure, defined here as $p_{rms} = \sqrt{\sum_i p_i^2/N}$ is shown in Fig. 12. The p_{rms} values obtained are higher for the higher air mass flow rate case indicating the instability in this case was higher. This is because for the higher air mass flow rate, the thermal energy in the system is higher. The shape of the temperature curve is as expected, even though it did not peaked at exactly a mean ϕ value of 1.0 due to possible measurement errors.

To investigate whether hysteresis was present in the 6 g/s case, the measurements were repeated. In order to monitor this behavior closely and catch the transition from stable to unstable behavior and vice versa, the pulsations levels were kept lower for the runs considered by increasing the damping in the system. The hysteresis loop obtained beginning from an equivalence ratio of 0.69 is shown in Fig. 13.

7 Conclusions

The stability map of the matrix burner obtained from measurements is discussed. The importance of the choice of the combustion model in thermoacustics simulations is highlighted followed by the investigation of non-linearities and its effect on the flame response to single frequency forcing. Also considered is the effect of the limit-cycle behavior on the choice of the actuator used in the control of combustion instabilities. Finally, the limit-cycle behavior is further investigated by keeping the average air mass fixed and gradually increasing the fuel mass flow rate. In one of the cases considered, the system

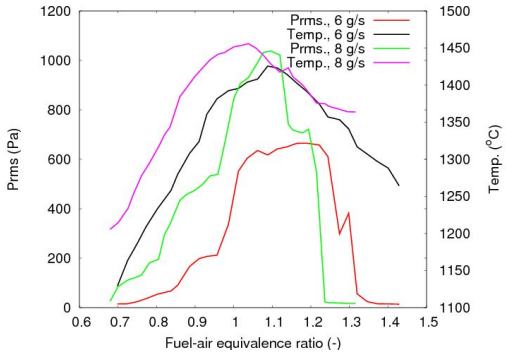

Figure 12: Variation of p_{rms} and Temperature with Equivalence Ratio.

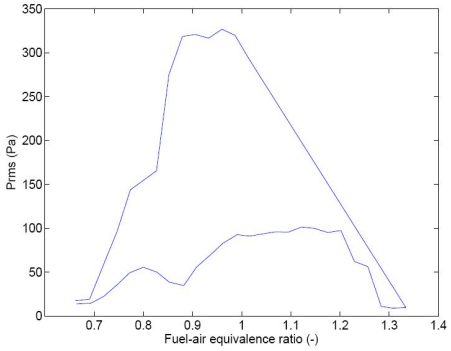

Figure 13: Plot of the hysteresis loop obtained in the matrix burner.

bifurcated from stable to unstable when the fuel mass flow was gradually increased and from unstable to stable when the fuel flow was gradually decreased at the same equivalence ratio. In future work, the limit of non-linearity in the matrix burner will be investigated. Also, answers would be sought for whether the flame front interaction in the matrix burner is contributing to thermoacoustic instability.

Acknowledgments

The authors gratefully acknowledge the financial support of the Deutsche Forschungsgemeinschaft (DFG) within the Collaborative Research Center (SFB) 686 "Model based control of homogenized low-temperature combustion". The responsibility of the content of this publication lies with the authors.

References

[1] J. P. Hathout, M. Fleifil, A. M. Annaswamy, and A. F. Ghoniem. Combustion Instability Active Control Using Periodic Fuel Injection. *Journal of Propulsion and Power*, 18, 2002.

[2] J. Shinjo, S. Matsuyama, Y. Mizobuchi, and S. Ogawa. Study on Flame Dynamics with Secondary Fuel Injection Control by Large Eddy Simulation. *Combustion and Flame*, 150:277–291, 2007.

[3] A.A. Putnam. *Combustion Driven Oscillations in Industry*. American Elsevier Publishers, New York, 1971.

[4] T.J. Poinsot, A.C. Trouve, D.P. Veynante, S.M. Candel, and E.J. Esposito. Vortex-driven Acoustically Coupled Combustion Instabilities. *J. Fluid Mech.*, 177:265–292, 1987.

[5] M. Mettenleiter, F. Vuillot, and S. Candel. Numerical Simulation of Adaptive Control: Application to Unstable Solid Rocket Motors. *AIAA*, 40, May 2002.

[6] J.W.S. Rayleigh. The Explanation of Certain Acoustical Phenomenon. *Nature*, 18:319–321, 1878.

[7] T. Poinsot and D. Veynante. *Theoretical and Numerical Combustion*. Edwards, second edition, 2005.

[8] B.T. Chu. On the Energy Transfer to Small Disturbances in Fluid Flow. *In Acta Mechanica, Wien: Springer*, 1:215–234, 1964.

[9] K. Kalyanaraman. At 340 MW, a powerhouse. *Turbomachinery International*, 8, 2007.

[10] D.J. Cook, H. Pitsch, and N. Peters. Numerical Simulation of Combustion Instabilities in a Lean Premixed Combustor with Finite Rate Chemistry. *ASME TURBO EXPO, Atlanta Georgia, Paper GT2003-38558*, June 16-19 2003.

[11] A. Banaszuk, C.A. Jacobson, A. I. Khibnik, and P.G. Mehta. Linear and Non-linear Analysis of Controlled Combustion Processes. Part I: Linear Analysis. *Proceedings of the 1999 IEEE International Conference on Control Applications*, August 22-27 1999.

[12] A. Banaszuk, C.A. Jacobson, A.I. Khibnik, and P.G. Mehta. Linear and Non-linear Analysis of Controlled Combustion Processes. Part II: Noninear Analysis. *Proceedings of the 1999 IEEE International Conference on Control Applications*, 1999.

[13] T. Lieuwen and B.T. Zinn. Experimental Investigation of Limit Cycle Oscillations in an Unstable Gas Turbine Combustor. 38^{th} *ASIA Aerospace Sciences Meeting, Reno, NV, ASIA 2000-0707*, January 2000.

[14] G. Isella, C. Seywert, F.E.C. Culick, and E.E. Zukoski. A Further Note on Active Control of Combustion Instabilities Based on Hyseresis. *Short Communication, Combustion Science and Technology*, 127:381–388, 1997.

[15] G.A. Richards, M. Janus, and E.H. Robey. Control of Flame Oscillations with Equivalence Ratio Modulation. *Journal of Propulsion and Power*, 15:232–240, 1999.

[16] J. Lepers, W. Krebs, B. Prade, P. Flohr, G. Pollarolo, and A. Ferrante. Investigation of Thermoacoustic Stability Limits of an Annular Gas Turbine Combustor Test-Rig. *ASME TURBO EXPO, Reno-Tahoe, Nevada, USA, Paper GT2005-68246*, June 6-9 2005.

[17] K.I. Matveev and F.E.C. Culick. A Study of Transitionmodel to Instability in a Rijke Tube with Axial Temperature Gradient. *Sound and Vibration*, 264(3):689–706, 2003.

[18] E. Deuker. *Ein Beitrag zur Vorausberechnung des askustischen Stabilitätsverhaltens von Gasturbinen-Brennkammern mittels theoretischer und experimenteller Analyse von Brennkammerschwingungen.* PhD thesis, Fakultät für Maschinenwesen der Rheinisch-Westfälischen Technischen Hochschule Aachen, 1995. Published in VDI Verlag, Energietechnik, Reihe 6, Nr. 317.

[19] U. Krüger. *Experimentelle und Numerische Untersuchungen zur Flammendynamik.* PhD thesis, Fakultät für Maschinenwesen der Rheinisch-Westfälischen Technischen Hochschule Aachen, 1998.

[20] A.H. Lefebvre. *Gas Turbine Combustion.* McGraw-Hill Series in Energy, Combustion, and Environment. McGraw-Hill, 1983.

[21] D. Bohn, N. Ohlendorf, and J.F. Willie. Phase Shift Control of Combustion Instability in a Gas Turbine Matrix Burner Using Acoustic Forcing and Pulsed Fuel Injection. *ASME TURBO EXPO, Orlando, Florida, USA, Paper GT2009-59083*, June 8-12 2009.

[22] B. Schuermans, H. Luebcke, D. Bajusz, and P. Flohr. Thermoacoustic Analysis of Gas Turbine Combustion Systems Using Unsteady CFD. *ASME TURBO EXPO, Reno-Tahoe, Nevada, Paper GT2005-6839*, June 6-9 2005.

[23] N. Peters. *Turbulent Combustion: The State of the Art.* Cambridge University Press, May 2000.

[24] C.K. Westbrook and F.L. Dryer. Simplified Reaction Mechanisms for the Oxidisation of Hydrocarbon Fuel in Flames. *Combustion Science and Technology.*, 27:31–43, 1981.

[25] C.K. Westbrook and F.L. Dryer. Chemical Kinetic Modelling of Hydrocarbon Combustion. *Prog. Energy Combustion Sci.*, 10:1–57, 1984.

[26] D. Bohn and E. Deuker. An Acoustical Model to Predict Combustion Driven Oscillations. 20^{th} *International Congress on Combustion Engines*, 1993.